Crystal Structure and Optical Properties of a Chiral Mixed Thiolate/Stibine-Protected Au_{18} Cluster

Justin B. Patty,[†] Shana Havenridge,[§] Dylan Tietje-Mckinney,[†] Maxime A. Siegler,[‡] Kundan K. Singh,[†] Roumina Hajy Hosseini,[†] Mohamed Ghabin,[†] Christine M. Aikens,[§*] and Anindita Das[†*]

[†] Department of Chemistry, Southern Methodist University, Dallas, Texas 75275, United States
[§] Department of Chemistry, Kansas State University, Manhattan, Kansas 66506, United States
[‡] Department of Chemistry, Johns Hopkins University, Baltimore, Maryland 21218, United States

Abstract

We report the first example of a chiral mixed thiolate/stibine-protected gold cluster, formulated as $Au_{18}(S\text{-}Adm)_8(SbPh_3)_4Br_2$ (where S-Adm = 1-adamantanethiolate). Single crystal X-ray crystallography reveals the origin of chirality in the cluster to be the introduction of the rotating arrangement of $Au_2(S\text{-}Adm)_3$ and $Au(S\text{-}Adm)_2$ staple motifs on an achiral Au_{13} core, and the subsequent capping of the remaining gold atoms by $SbPh_3$ and Br^- ligands. Interestingly, the structure and properties of this new Au_{18} cluster are found to be different from other reported achiral Au_{18} clusters and the only other stibine-protected $[Au_{13}(SbPh_3)_8Cl_4]^+$ cluster. Detailed analyses on the geometric and electronic structures of the new cluster are carried out to gain insights into its optical properties as well as reactivity and stability of such mixed-monolayer protected clusters.

Introduction

Monolayer-protected metal clusters, consisting of a precise number of metal atoms and ligands, lie at the interface of small molecules and bulk metal and have recently emerged as a new frontier in colloidal nanoscience. Gold clusters, in particular, act as paradigm systems due to their extraordinary stability, unique geometric structures and physicochemical properties, and hence are commonly referred to as "superatoms" or magic-sized clusters.[1-3] Since the pioneering crystal structure determination of a $Au_{102}(SR)_{44}$ cluster by Kornberg in 2007,[4] several thiolate- and

alkynyl-protected Au cluster superatoms, containing tens to hundreds of Au atoms, have been reported.[5-10] In parallel, phosphine-protected Au clusters have attracted renewed interest since the early reports dating back to the late 1960s.[11-15]

Among the various structurally-resolved Au clusters, the Au_{11} and Au_{13} icosahedral superatom structural motifs are frequently encountered,[1] both as (1) structures of standalone clusters directly protected by ligands, e.g., $[Au_{13}(dppe)_5Cl_2]^{2+}$ (where dppe = 1,2-bis(diphenylphosphino)ethane),[12] $Au_{11}(PPh_3)_7Cl_3$,[13] etc.; or by the staple motifs exhibited by thiolate- and alkyne-protected clusters (e.g., core-shell Au_{25} clusters)[16-18], and (2) structurally fused units in larger clusters. For example, a "cluster of clusters" motif has been previously described in biicosahedral Au_{25},[19] triicosahedral Au_{37},[20] and pentaicosahedral Au_{60} clusters[21] (co-protected by phosphines and thiolates/selenolates/alkynes) through the sharing of vertex Au atoms of the icosahedral Au_{13} units. Additionally, edge- and face-sharing modes of cluster growth have been identified using the Au_{13} core, which can itself be viewed as being composed of 20 tetrahedra and hence, can exhibit considerable distortions in certain clusters.[22-25,38] Very recently, N-heterocyclic carbenes (NHCs), with stronger s-donor properties as compared to analogous phosphines, have been used to synthesize stable Au_{13} and Au_{25} clusters based on the Au_{13} core.[26-28] On the other hand, Au clusters protected by heavier phosphine-analogues such as stibines are severely underdeveloped, despite these ligands exhibiting unique coordination and reactivity features in Au(I) complexes at the molecular scale.[29] Given these attractive characteristics, it is surprising to note that stibines have not been widely used for making materials at the nanoscale and to the best of our knowledge, even to make materials at larger length scales such as self-assembled monolayers (SAMs). With the lone exception of a $[Au_{13}(SbPh_3)_8Cl_4]^+$ cluster reported in 2018, no other reports on stibine-based gold clusters currently exist.[30] A major reason for this is believed to be the weaker coordinating ability of stibines as compared to phosphines due to their diffuse donor orbitals.

In this work, we report the first example of a mixed thiolate/stibine-protected Au cluster containing 18 Au atoms. The crystal structure of the new charge-neutral, chiral cluster formulated as $Au_{18}(S\text{-}Adm)_8(SbPh_3)_4Br_2$, (S-Adm = 1-adamantanethiolate), features an icosahedral Au_{13} core protected by a pair of $Au_2(S\text{-}Adm)_3$ dimeric and one $Au(S\text{-}Adm)_2$ monomeric staple motifs, in

addition to four coordinated $SbPh_3$ ligands and two Br^- ions (Figure 1). By comparing this new cluster's properties with previously reported stibine-protected $[Au_{13}(SbPh_3)_8Cl_4]^+$,[30] and thiolate-protected $Au_{18}(SC_6H_{11})_{14}$ clusters,[37,39] we demonstrate for the first time that the properties and stability of stibine-based Au clusters can be tailored at the atomic level by employing a mixed-ligand approach. These insights are not only expected to broadly expand the use of stibine-based ligands at larger length scales, but also provide key design rules in mixed ligand-mediated tuning of surface properties of nanomaterials.

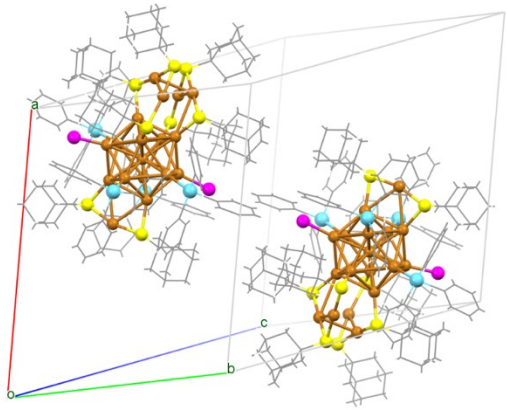

Figure 1. Crystal packing in the unit cell of the $[Au_{18}(S\text{-}Adm)_8(SbPh_3)_4Br_2]^0$ structure. The unit cell contains a pair of left- and right-handed isomers, as the structure is centrosymmetric. (Color labels: Brown = Au; yellow = S; blue = Sb, pink = Br, grey = C, H are omitted for clarity).

Results and discussion

Synthesis and Structure Determination

The synthesis of the $Au_{18}(S\text{-}Adm)_8(SbPh_3)_4Br_2$ cluster involves two primary steps: (1) synthesis of the stibine-protected $[Au_{13}(SbPh_3)_8Br_4]^+$ cluster (which is structurally similar to the previously reported $[Au_{13}(SbPh_3)_8Cl_4]^+$ cluster),[30] and (2) addition of excess 1-adamantanethiol to convert it to the mixed thiolate/stibine-protected Au_{18} cluster. Details of the synthesis are provided in the Supporting Information. Single crystal growth of the clusters was achieved by vapor diffusion of pentane into a dichloromethane solution of the crude product, followed by structure determination by single crystal X-ray crystallography.

The crystal structure of the $Au_{18}(S\text{-}Adm)_8(SbPh_3)_4Br_2$ cluster is best described in the centrosymmetric triclinic space group $P\bar{1}$, with the unit cell comprising a pair of enantiomers exhibiting quasi-C_2 symmetry (Figure 1). The kernel of the cluster is a Au_{13} icosahedron (Figure 2A), like the core of the previously reported stibine-protected $[Au_{13}(SbPh_3)_8Cl_4]^+$ cluster,[30] which, in turn, is protected by three kinds of ligands. Starting with thiolates, we find a pair of closely-

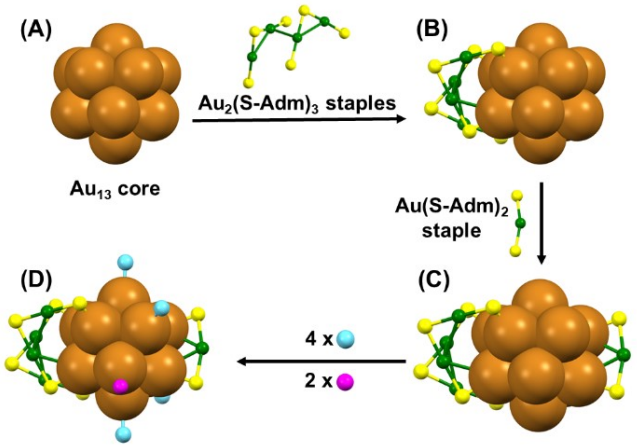

Figure 2. Anatomy of the $Au_{18}(S\text{-}Adm)_8(SbPh_3)_4Br_2$ cluster, starting with the icosahedral Au_{13} kernel (A); addition of two dimeric staggered staple motifs and one monomeric staple motif gives rise to (B) and (C) respectively, followed by the addition of stibine and bromide ligands to remaining Au atoms, yielding the $Au_{18}(S\text{-}Adm)_8(SbPh_3)_4Br_2$ cluster (D). (Color labels: brown/green = Au; yellow = S; blue = Sb, pink = Br, carbon tails of triphenylstibine and 1-adamantanethiolate ligands are omitted for clarity).

spaced, staggered $Au_2(S\text{-}Adm)_3$ dimeric staple motifs (closest Au-Au distance between the dimers is 2.963 Å, Figure 2B) and one $Au(S\text{-}Adm)_2$ monomeric staple motif, directly opposite to the pair of dimers (Figure 2C). The remaining 6 exposed Au atoms are further capped by 4 triphenylstibine and 2 bromide ions (Figure 2D). We further performed electrospray ionization mass spectrometric analysis (ESI-MS) and NMR spectroscopy to confirm the mass and surface ligand composition of the $Au_{18}(S\text{-}Adm)_8(SbPh_3)_4Br_2$ cluster, respectively (Figures S5-S7).

Interestingly, the pair of staggered dimers and a monomeric staple motif in the Au_{18}(S-Adm)$_8$($SbPh_3$)$_4Br_2$ cluster structure are reminiscent of the widely studied chiral $Au_{38}(SR)_{24}$ clusters, the structure of which features staggered dimeric staple motifs on a face-fused biicosahedral-based Au core, leading to its chiral nature.[23,31-33] Apart from using chiral protecting ligands, chirality in NCs can be typically induced in two ways: (1) presence of an inherent chiral Au core,[34,35] and (2) chiral arrangement of ligand-binding modes or "staple motifs" around an achiral Au core.[18,23] Additionally, it has been observed that chirality predominantly originates from the rotating arrangement of multiple staple motifs in chiral thiolate-protected Au clusters.[33] Hence, we believe that the introduction of Au-thiolate staple motifs and subsequent capping of the remaining Au atoms by $SbPh_3$ and Br^- ligands is the key to breaking the symmetry of the achiral Au_{13} core in the Au_{18}(S-Adm)$_8$($SbPh_3$)$_4Br_2$ cluster (Figure 3).

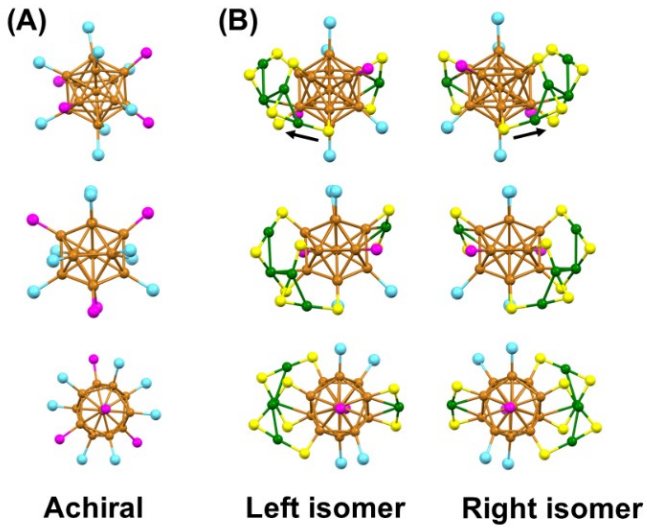

Figure 3. Total structures of triphenylstibine-based Au clusters in different orientations; (A) $[Au_{13}(SbPh_3)_8X_4]^+$(X=Cl/Br);(B) the two enantiomers of Au_{18}(S-Adm)$_8$($SbPh_3$)$_4Br_2$ (Color labels: brown/green = Au; yellow = S; blue = Sb, pink = Br/Cl, carbon tails of triphenylstibine and 1-adamantanethiolate are omitted for clarity).

It is also worthy to comment on the crystal structures of the other reported ligand-protected Au_{18} clusters. Unlike the icosahedral Au_{13} core in the Au_{18}(S-Adm)$_8$($SbPh_3$)$_4Br_2$ cluster (Figure 4A), the Au core of a diphosphine-protected $[Au_{18}(dppm)_6X_4]^{2+/4+}$ (X=Cl/Br) cluster can be

envisioned as a bi-capped bioctahedral Au_{18} core (Figure 4B),[24] or the fusion of two distorted Au_{11} incomplete icosahedra by sharing a common Au_4 face.[25] On the other hand, a fully thiolate-protected $Au_{18}(SC_6H_{11})_{14}$ was found to contain a face-fused bioctahedral Au_9 core, where two distorted Au_6 octahedra were assembled together by sharing a common Au_3 face (Figure 4C).[36,37,39] This indicates the critical role of different kinds of ligands in determining and stabilizing the highly diverse Au cores of clusters in this size regime.[1,2,38-40]

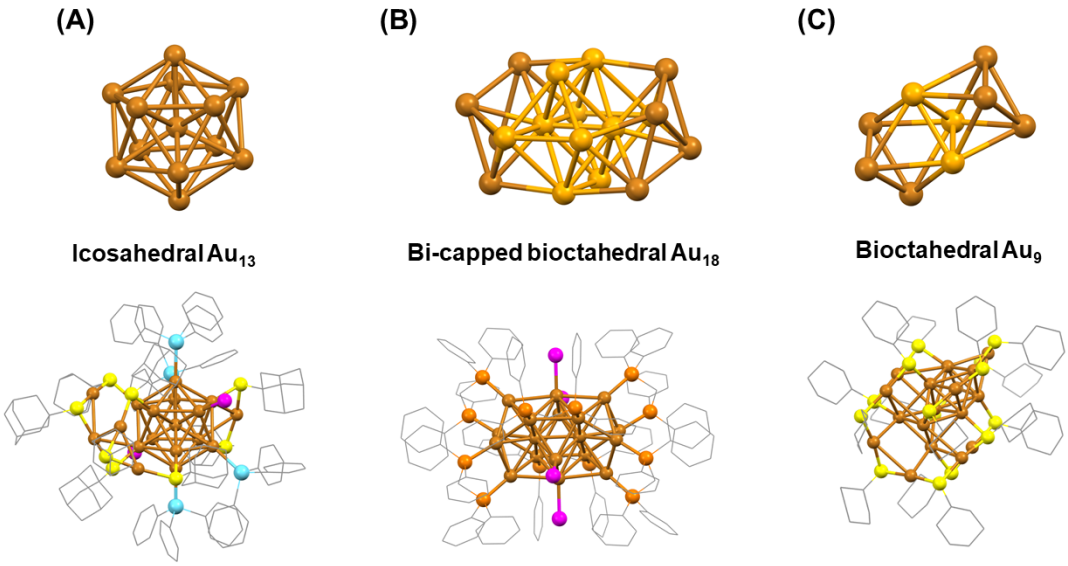

Figure 4. Experimentally determined Au cores and total structures of ligand-protected Au_{18} clusters: (A) $Au_{18}(S\text{-}Adm)_8(SbPh_3)_4Br_2$, (B) $[Au_{18}(dppm)_6X_4]^{2+/4}$ (X=Cl/Br), and (C) $Au_{18}(SC_6H_{11})_{14}$. (Color labels: brown/mustard = Au; yellow = S; blue = Sb, pink = Br/Cl, orange = P; gray = C).

Theoretical Analysis of Optical and Chiroptical Properties

To achieve insights into the electronic structure of the $Au_{18}(S\text{-}Adm)_8(SbPh_3)_4Br_2$ cluster, density functional theory (DFT) calculations were carried out at the B3LYP/DZ level of theory (see Supplementary Information for details), where the bond distances were maintained at the geometry indicated by the crystal structure. The Right isomer (Figure 3B) of the cluster was also optimized at the BP86-D3/DZ and Xalpha/TZP levels of theory. As there are no notable

differences in the absorption spectra between the optimized and unoptimized clusters, the analysis was done with the bond distances maintained by the average length represented in the crystal structure of the cluster. The crystal structure of $Au_{18}(S\text{-}Adm)_8(SbPh_3)_4Br_2$ demonstrates that the average Au-Sb bond is 2.549 ± 0.027 Å and the average Au-Br bond is 2.437 ± 0.001 Å. These bonds are slightly larger than the average Au-S bonds in the cluster which are 2.338 ± 0.072 Å. To understand how the electronic density distribution changes in terms of atomic charges (due to Au-ligand interactions) within the $Au_{18}(S\text{-}Adm)_8(SbPh_3)_4Br_2$ cluster, a Hirschfield charge analysis was carried out. Herein, all the Sb atoms are found to possess an approximate +0.47 partial charge, while Br atoms possess partial charges of approximately -0.17. The sulfur atoms stay neutral in all except two positions, where the partial charge increases to +0.02.

Figures 5 and 6A show the experimental and theoretical optical absorption spectra of the $Au_{18}(S\text{-}Adm)_8(SbPh_3)_4Br_2$ cluster, respectively. The theoretical absorption spectrum of the cluster

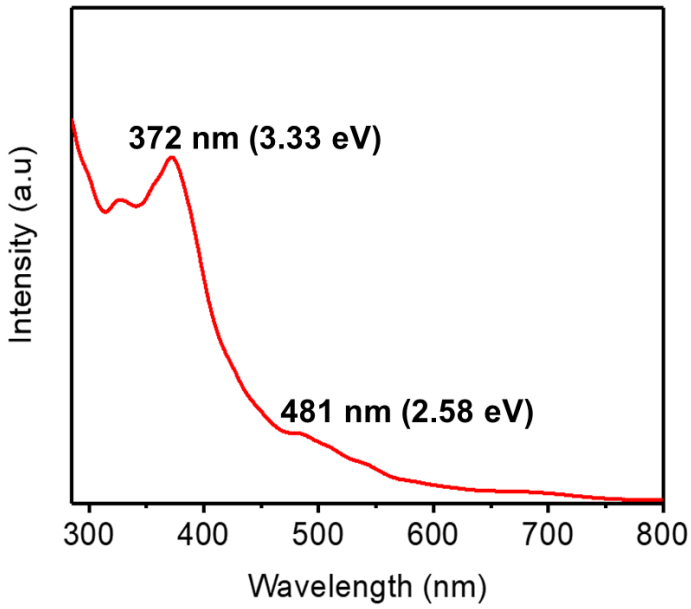

Figure 5. Experimental UV-visible absorption spectrum of the $Au_{18}(S\text{-}Adm)_8(SbPh_3)_4Br_2$ cluster. The most prominent peak appears at 372 nm.

at the B3LYP/DZ level of theory shows a broad peak at 363 nm (3.41 eV) with an oscillator strength of 0.1027 a.u. In addition to the main peak, there is a shoulder at 3.10 eV with an oscillator strength of 0.0721 a.u.

$Au_{18}(S\text{-}Adm)_8(SbPh_3)_4Br_2$ possesses a set of unique optical properties that slightly differs from that of pure thiolate-protected Au_{18} clusters and $[Au_{18}(dppm)_6Cl_4]^{4+}$.[24, 36-37] In the low energy region, three peaks are seen in the theoretical spectrum at 512 nm, 558 nm and 600 nm; these peaks have oscillator strengths below 0.002 a.u. The transitions responsible for these three peaks take place in the core of the nanoparticle, all showing superatomic P → D nature where the main transitions occur between HOMO → LUMO+4, HOMO → LUMO+3 and HOMO → LUMO, respectively. These peaks, however, have much lower oscillator strengths than the most prominent absorption peak in the spectrum, which are found to arise from ligand-based transitions.

The main peak of interest occurs at 3.41 eV in the calculations and only slightly overestimates the experimental peak at 372 nm (3.33 eV). This peak is made up of two dominant

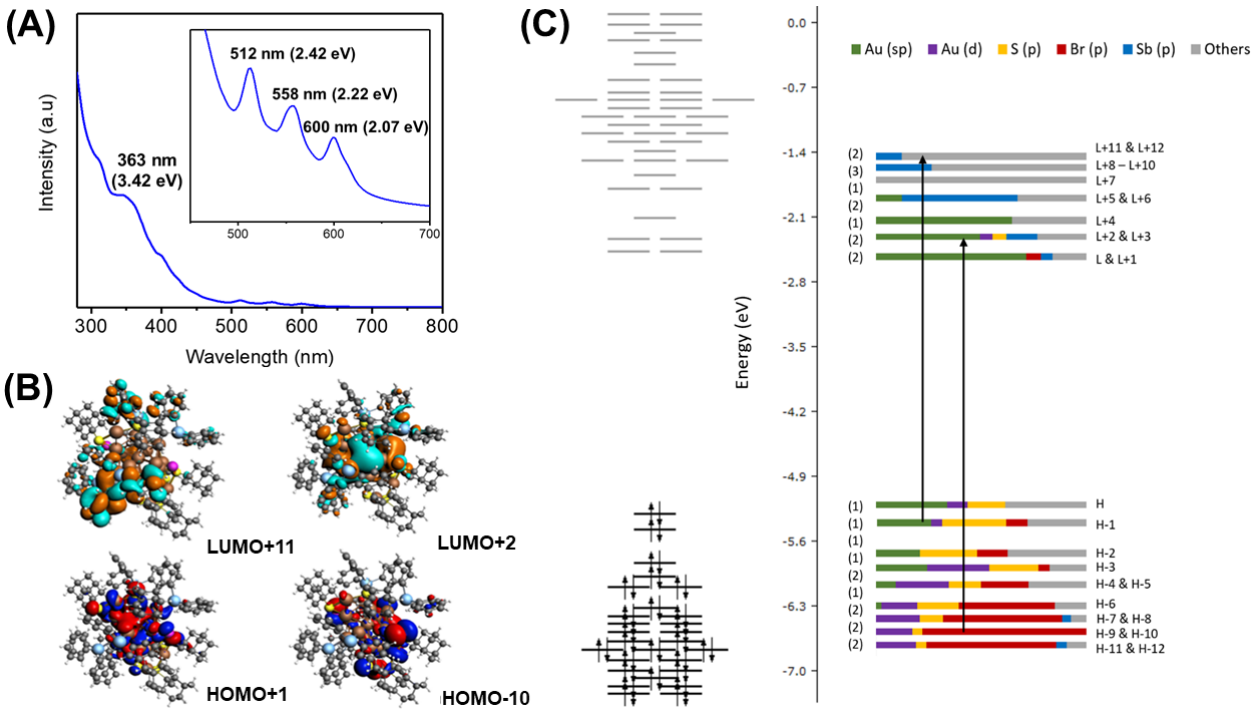

Figure 6. (A) Theoretical optical spectrum of the $Au_{18}(S\text{-}Adm)_8(SbPh_3)_4Br_2$ cluster (Inset: zoomed-in optical spectrum of the $Au_{18}(S\text{-}Adm)_8(SbPh_3)_4Br_2$ cluster in the low energy region) ; (B) Molecular orbitals (MOs) of $Au_{18}(S\text{-}Adm)_8(SbPh_3)_4Br_2$ at the B3LYP/DZ level of theory that contribute to the peak at 363 nm (3.41 eV). (Color labels: brown = Au; yellow = S; blue = Sb, pink = Br, grey = C, white = H) (C) Molecular orbital diagram and contributing atomic orbitals of $Au_{18}(S\text{-}Adm)_8(SbPh_3)_4Br_2$ at the B3LYP/DZ level of theory. The number of degenerate MOs at a specific energy is in parenthesis.

transitions, HOMO-10→ LUMO+2 and HOMO-1→ LUMO+11; the orbitals involved in these transitions are provided in Figure 6B. The first transition is HOMO-1→ LUMO+11, which arises from an electronic transition out of an occupied superatomic P shaped orbital in the icosahedral core of the cluster to an antibonding orbital comprised of the π* orbitals on the phenyl rings of the $SbPh_3$ ligands. The second dominant transition, HOMO-10→ LUMO+2, arises from an occupied orbital that primarily consists of individual p_x and p_y orbitals residing mostly around the bromine atoms, with little contribution from the sulfur p orbitals across the -S-Au-S- staple motifs. The electronic transition occurs into a superatomic D_z^2 shaped orbital in the icosahedral core of the Au_{18} cluster. These transitions show that the electronic density corresponding to the main absorption peak includes both core→ ligand and ligand→ core contributions. Other levels of theory have been analyzed, and the qualitative results of the transitions that correspond to the main absorption peak remain the same. The molecular orbital (MO) diagram for this nanocluster is shown in Figure 6C. At the B3LYP/DZ level of theory, the HOMO-LUMO gap of the nanocluster at the crystal structure geometry is 2.82 eV. It is important to note that the HOMO-LUMO gap and the first excited state energy (i.e., the optical gap) can differ. Although the first excited state is often dominated by the HOMO to LUMO transition, it is not always the principal transition (in this case, the peak at 2.02 eV arises from HOMO-LUMO+1, with contributions from the HOMO-LUMO and HOMO-LUMO+2). Most importantly, several transitions mix together to yield an excited state, and this can reduce the energy of the state due to configuration interaction.

As shown in Figure S1, the HOMO, HOMO-1 and HOMO-2 MOs show superatomic P type character in the core of the nanoparticle. These orbitals have relative energies of 0.00 eV, -0.16 eV and -0.53 eV respectively. The frontier orbitals of this cluster are highly delocalized from s contributions in the gold core. Though different cluster geometries may lead to orbital morphologies with nondegeneracies due to breaking of spherical symmetry, they can still be classified as superatomic orbitals.[41,42] As an example, in clusters such as $Au_{11}(dpb)_4Cl_2^+$, the HOMO-2 orbital is 0.44 eV lower in energy than the HOMO, but still shows superatomic P type nature.[41] As an additional comparison, the superatomic P orbitals in thiolated clusters are much closer to degeneracy, differing only around 0.03 eV.[17] The HOMO-3 and HOMO-4 orbitals are primarily based around the two $Au_2(S\text{-}Adm)_3$ staple motifs with minimal contribution from the third $Au(S\text{-}Adm)_2$ monomeric motif on the other side of the Au_{18} cluster. HOMO-5 through HOMO-8 are primarily ligand-based, arising from the p orbitals on Br as well as the p orbitals

from Au and S that are concentrated around the dimeric and monomeric Au-thiolate staple motifs, with no contribution from the Sb atoms. Small contributions start to appear from the Sb atoms in the HOMO-9 orbital. Further, LUMO through LUMO+4 correspond to superatomic D orbitals in the core of the Au_{18} cluster. The antibonding character in the ligands starts to show in the LUMO+6, which is comprised of π* orbitals on the phenyl rings of the $SbPh_3$ ligands.

To probe the chirality of the $Au_{18}(S\text{-}Adm)_8(SbPh_3)_8Br_2$ cluster, the computed circular dichroism (CD) spectra of the Au_{13} core as well as the total $Au_{18}(S\text{-}Adm)_8(SbPh_3)_4Br_2$ are shown in Figure 7. As Au atoms in the core are not in their most symmetric locations due to their interactions with the ligands, there is still a small intensity from the Au_{13} core (blue curve, Figure 7). However, the signal from the full Au_{18} cluster is significantly more intense (red curve, Figure 7), confirming the chirality of the $Au_{18}(S\text{-}Adm)_8(SbPh_3)_8Br_2$ originates from the ligand shell of the cluster.

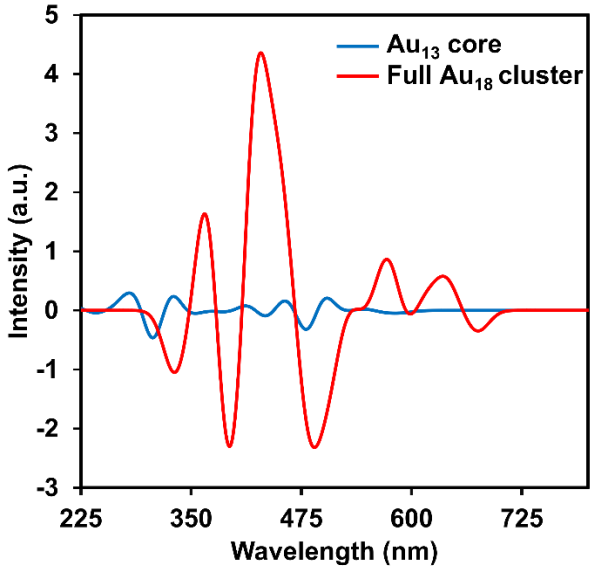

Figure 7. Calculated CD spectra of both the full Au_{18} cluster (right isomer) as well as the Au_{13} core alone at the BP86/DZ level of theory.

Stability and Reactivity Studies

Finally, we compared the stability and reactivity of the new mixed thiolate/stibine-protected $Au_{18}(S\text{-}Adm)_8(SbPh_3)_4Br_2$ cluster with that of the only stibine-protected

$[Au_{13}(SbPh_3)_8X_4]^+$ (X=Cl/Br) cluster and a fully thiolate protected $Au_{18}(SC_6H_{11})_{14}$ cluster to study the effects of Au-thiolate staple motif incorporation in stibine-based gold clusters (Figures 8 and S11). Previously, the $[Au_{13}(SbPh_3)_8Cl_4]^+$cluster has been shown to readily convert to a water-soluble $Au_{25}(SG)_{18}$ cluster, when reacted with excess glutathione (GSH) in a two-phase reaction.[30] Compared to analogous phosphine-protected Au_{11} clusters, this two-phase ligand exchange reaction with glutathione was found to be considerably faster in the case of the $[Au_{13}(SbPh_3)_8Cl_4]^+$ cluster, primarily due to the weaker coordinating ability of the stibine ligands which make this cluster less stable and hence, more prone to ligand exchange.[13,30] Interestingly, under the same reaction conditions, the $Au_{18}(SC_6H_{11})_{14}$ and $Au_{18}(S\text{-}Adm)_8(SbPh_3)_4Br_2$ clusters exhibited no ligand exchange with glutathione and retained their intact structures in the organic phase (Figure 8), thereby demonstrating the protective role of the Au-thiolate staple motifs in stabilizing the mixed ligand-protected $Au_{18}(S\text{-}Adm)_8(SbPh_3)_4Br_2$ cluster structure during this ligand exchange reaction. We next tested the thermal stability as well as the stability of the three clusters under oxidizing and reducing conditions (Figure S9). Herein, the $Au_{18}(SC_6H_{11})_{14}$ cluster is found to be the most

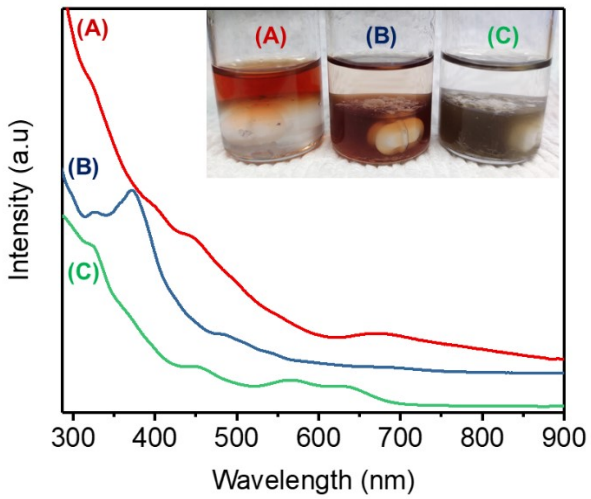

Figure 8. UV–vis spectra of the products of the two-phase ligand exchange reaction with excess glutathione; (A) the $[Au_{13}(SbPh_3)_8X_4]^+$ (X=Cl/Br) cluster converts to a water- soluble $Au_{25}(SG)_{18}$ cluster within 30 minutes (red trace), while (B) the $Au_{18}(S\text{-}Adm)_8(SbPh_3)_4Br_2$, and (C) $Au_{18}(SC_6H_{11})_{14}$ clusters remain intact in the organic phase (blue and green traces, respectively). Inset: Pictures of the two-phase reaction mixtures of (A) $[Au_{13}(SbPh_3)_8Br_4]^+$, (B) $Au_{18}(S\text{-}Adm)_8(SbPh_3)_4Br_2$, and (C) $Au_{18}(SC_6H_{11})_{14}$ clusters.

stable under the tested conditions, followed by $Au_{18}(S\text{-}Adm)_8(SbPh_3)_4Br_2$ cluster, which for instance, is found to be robust under reducing conditions unlike the $[Au_{13}(SbPh_3)_8Br_4]^+$ cluster. Overall, these results underscore the importance of the ligand shell in dictating and modifying the observed properties of metal clusters.

Conclusion

We have synthesized and experimentally determined the crystal structure of a new mixed thiolate/stibine-protected $Au_{18}(S\text{-}Adm)_8(SbPh_3)_4Br_2$ cluster, the properties of which are found to be very different from the only previous stibine-protected $[Au_{13}(SbPh_3)_8Cl_4]^+$ cluster. Specifically, the incorporation of dimeric and monomeric Au-thiolate staple motifs in the $Au_{18}(S\text{-}Adm)_8(SbPh_3)_4Br_2$ structure is found to (1) induce chirality by breaking the symmetry of the achiral Au_{13} core, thereby indicating that chirality can be engendered in achiral clusters protected by electroneutral ligands such as PPh_3 and $SbPh_3$, through generation of Au-thiolate staple motifs on their surfaces, and (2) enhance the stability of clusters by resisting ligand exchange in the presence of excess glutathione. Our results not only underscore the importance of the ligand shell in tailoring the observed properties of closely-related clusters but also inform that a mixed-ligand strategy may be used to synthesize stable metal clusters with weakly coordinating ligands such as $SbPh_3$. This knowledge is expected to spur the development of such mixed ligand-protected metal clusters with new properties and help gain critical insights into the effects of mixed-monolayer ligand shells on the stability and reactivity of metal nanoparticles.

Supporting Information

Details of the synthesis, X-ray crystallographic analysis, Computational details, and supporting Figures S1-9. This material is available free of charge via the Internet at http://pubs.acs.org.

AUTHOR INFORMATION

Corresponding Author

Email: aninditad@smu.edu (experiment); cmaikens@ksu.edu (theory)

ACKNOWLEDGMENT

A.D. thanks Southern Methodist University for start-up funds. S.H. and C.M.A. were supported by the National Science Foundation (CHE-1905048) of the United States. The computing for this work was performed on the Beocat Research Cluster at Kansas State University, which is funded in part by NSF grants CHE-1726332, CNS-1006860, EPS-1006860, and EPS-0919443.

REFERENCES

(1) Takano, S.; Tsukuda, T. Chemically Modified Gold/Silver Superatoms as Artificial Elements at Nanoscale: Design Principles and Synthesis Challenges. *J. Am. Chem. Soc.* **2021**, *143*, 1683–1698.

(2) Jin, R.; Zeng, C.; Zhou, M.; Chen, Y. Atomically Precise Colloidal Metal Nanoclusters and Nanoparticles: Fundamentals and Opportunities. *Chem. Rev.* **2016**, *116*, 10346−10413.

(3) Walter, M.; Akola, J.; Lopez-Acevedo, O.; Jadzinsky, P. D.; Calero, G.; Ackerson, C. J.; Whetten, R. L.; Grönbeck, H.; Hakkinen, H. A unified view of ligand-protected gold clusters as superatom complexes. *Proc. Natl. Acad. Sci. U. S. A.* **2008**, *105*, 9157−9162.

(4) Jadzinsky, P. D., Calero, G., Ackerson, C. J., Bushnell, D. A. & Kornberg, R. D. Structure of a thiol monolayer-protected gold nanoparticle at 1.1 Å resolution. *Science* **2007**, *318*, 430-433.

(5) Lei, Z.; Wan,X. -K.; Yuan, S. -F.; Guan, Z. -J.; Wang, Q, -M. Alkynyl Approach toward the Protection of Metal Nanoclusters. *Acc. Chem. Res.* **2018**, *51*, 2465–2474.

(6) Kang, X.; Zhu, M. Structural Isomerism in Atomically Precise Nanoclusters. *Chem. Mater.* **2021**, 33, 39–62.

(7) Aikens, C. M. Electronic and Geometric Structure, Optical Properties, and Excited State Behavior in Atomically Precise Thiolate-Stabilized Noble Metal Nanoclusters. *Acc. Chem. Res.* **2018**, *51*, 3065–3073.

(8) Sakthivel, N. A.; Dass, A. Aromatic Thiolate-Protected Series of Gold Nanomolecules and a Contrary Structural Trend in Size Evolution. *Acc. Chem. Res.* **2018**, *51*, 1774–1783.

(9) Hosier, C. A.; Anderson, I. D.; Ackerson, C. J. Acetylide-for-thiolate and thiolate-for-acetylide exchange on gold nanoclusters. *Nanoscale* **2020**,*12*, 6239-6242.

(10) Yao, Q.; Chen, T.; Yuan, X.; Xie, J. Toward Total Synthesis of Thiolate-Protected Metal Nanoclusters. *Acc. Chem. Res.* **2018**, 51, 1338– 1348.

(11) McPartlin, M.; Mason, R.; Malatesta, L. Novel cluster complexes of gold(0)–gold(I). *J. Chem. Soc. D: Chem. Commun.* **1969**, 334-334.

(12) Shichibu, Y.; Konishi, K. HCl-Induced Nuclearity Convergence in Diphosphine-Protected Ultrasmall Gold Clusters: A Novel Synthetic Route to "Magic-Number" Au_{13} Clusters. *Small* **2010**, *11*, 1216-1220.

(13) McKenzie, L.C.; Zaikova, T. O.; Hutchison, J. E. Structurally Similar Triphenylphosphine-Stabilized Undecagolds, $Au_{11}(PPh_3)_7Cl_3$ and $[Au_{11}(PPh_3)_8Cl_2]Cl$, Exhibit Distinct Ligand Exchange Pathways with Glutathione. *J. Am. Chem. Soc.* **2014**, *136*, 13426–13435.

(14) Das, A., Li, T., Nobusada, K., Zeng, Q., Rosi, N. L.; Jin, R. Total Structure and Optical Properties of a Phosphine/Thiolate-Protected Au_{24} Nanocluster. *J. Am. Chem. Soc.* **2012**, *134*, 20286-20289.

(15) Zhang, S.-S.; Feng, L.; Senanayake, R. D.; Aikens, C. M.; Wang,X.-P.; Zhao, Q. -Q.; Tunga, C. -H.; Sun D. Diphosphine-Protected Ultrasmall Gold Nanoclusters: Opened Icosahedral Au_{13} and Heart-Shaped Au_8 Clusters. *Chem. Sci.*, **2018**, *9*, 1251-1258.

(16) Heaven, M. W.; Dass, A.; White, P. S.; Holt, K. M.; Murray, R. W. Crystal Structure of the Gold Nanoparticle $[N(C_8H_{17})_4][Au_{25}(SCH_2CH_2Ph)_{18}]$. *J. Am. Chem. Soc.* **2008**, *130*, 3754-3755.

(17) Zhu, M., Aikens, C. M., Hollander, F. J., Schatz, G. C. & Jin, R. Correlating the Crystal Structure of a Thiol-Protected Au_{25} Cluster and Optical Properties. *J. Am. Chem. Soc.* **2008**, *130*, 5883-5885.

(18) Li, J.-J.; Guan, Z.-J.; Lei, Z.; Hu, F.; Wang, Q.-M. Same Magic Number but Different Arrangement: Alkynyl-Protected Au_{25} with D_3 Symmetry. *Angew. Chem. Int. Ed.* **2019**, *58*, 1083–1087.

(19) Shichibu, Y.; Negishi, Y.; Watanabe, T.; Chaki, N. K.; Kawaguchi, H.; Tsukuda, T. Biicosahedral Gold Clusters $[Au_{25}(PPh_3)_{10}(SC_nH_{2n+1})_5Cl_2]^{2+}$ (n = 2−18): A Stepping Stone to Cluster-Assembled Materials. *J. Phys. Chem. C* **2007**, *111*, 7845-7847.

(20) Jin, R.; Liu, C.; Zhao, S.; Das, A.; Xing, H.; Gayathri, C.; Xing, Y.; Rosi, N. L.; Gil, R. R.; Jin, R. Tri-icosahedral Gold Nanocluster $[Au_{37}(PPh_3)_{10}(SC_2H_4Ph)_{10}X_2]^+$: Linear Assembly of Icosahedral Building Blocks. *ACS Nano* **2015**, *9*, 8530−8536.

(21) Song, Y.; Fu, F.; Zhang, J.; Chai, J.; Kang, X.; Li, P.; Li, S.; Zhou, H.; Zhu, M. The Magic Au_{60} Nanocluster: A New Cluster-Assembled Material with Five Au_{13} Building Blocks. *Angew. Chem. Int. Ed.* **2015**, *54*, 8430−8434.

(22) Wan, X.-K.; Lin, Z.-W.; Wang, Q.-M. Au_{20} Nanocluster Protected by Hemilabile Phosphines. *J. Am. Chem. Soc.* **2012**, *134*, 14750-14752.

(23) Qian, H.; Eckenhoff, W. T.; Zhu, Y.; Pintauer, T.; Jin, R. Total Structure Determination of Thiolate-Protected Au_{38} Nanoparticles. *J. Am. Chem. Soc.* **2010**, *132*, 8280-8281.

(24) S.-S. Zhang, R. D. Senanayake, Q.-Q. Zhao, H.-F. Su, C. M. Aikens, X.-P. Wang, C.-H.; Tung, D. Sun, and L.-S. Zheng, $[Au_{18}(dppm)_6Cl_4]^{4+}$: Phosphine-Protected Gold Nanocluster with Rich Charge States. *Dalton Trans.* **2019**, *48*, 3635-3640.

(25) Jin, S.; Du, W.; Shuxin Wang, S.; Kang, X.; Chen, M.; Hu, D.; Chen, S.; Zou, X.; Sun, G.; Zhu, M. Thiol-Induced Synthesis of Phosphine-Protected Gold Nanoclusters with Atomic Precision and Controlling the Structure by Ligand/Metal Engineering. *Inorg. Chem.* **2017**, *56*, 11151–11159.

(26) Narouz, M. R.; Takano, S.; Lummis, P. A.; Levchenko, T. I.; Nazemi, A.; Kaappa, S.; Malola, S.; Yousefalizadeh, G.; Calhoun, L. A.; Stamplecoskie, K. G.; Häkkinen, H.; Tsukuda, T.; Crudden, C. M. Robust, Highly Luminescent Au_{13} Superatoms Protected by N-Heterocyclic Carbenes. *J. Am. Chem. Soc.* **2019**, *141*, 14997.

(27) Shen, H.; Xiang, S.; Xu, Z.; Liu, C.; Li, X.; Sun, C.; Lin, S.; Teo, B. K.; Zheng, N. Superatomic Au_{13} clusters ligated by different N-heterocyclic carbenes and their ligand-dependent catalysis, photoluminescence, and proton sensitivity. *Nano Res.* **2020**, *13*, 1908– 1911.

(28) Shen, H.; Deng, G.; Kaappa, S.; Tan, T.; Han, Y.-Z.; Malola, S.; Lin, S.-C.; Teo, B. K.; Häkkinen, H.; Zheng, N. Highly Robust but Surface-Active: An N-Heterocyclic Carbene-Stabilized Au_{25} Nanocluster. *Angew. Chem., Int. Ed.* **2019**, *58*, 17731– 17735.

(29) Jones, J. S.; Gabbaï, F. P. Coordination-and redox-noninnocent behavior of ambiphilic ligands containing antimony. *Acc. Chem. Res.* **2016**, *49*, 857–867.

(30) Li, Y. Z.; Ganguly, R.; Hong, K. Y.; Li, Y.; Tessensohn, M. E.; Webster, R.; Leong, W. K. Stibine-protected Au_{13} nanoclusters: syntheses, properties and facile conversion to GSH-protected Au_{25} nanocluster. *Chem. Sci.* **2018**, *9*, 8723– 8730.

(31) Dolamic, I.; Knoppe, S.; Dass, A.; Bürgi, T. First enantioseparation and circular dichroism spectra of Au_{38} clusters protected by achiral ligands. *Nat. Commun.* **2012**, *3*, 798.

(32) Knoppe, S.; Bürgi, T. Chirality in Thiolate-Protected Gold Clusters. *Acc. Chem. Res.* **2014**, *47*, 1318– 1326.

(33) Li, Y.; Higaki, T.; Du, X.; Jin, R. Chirality and Surface Bonding Correlation in Atomically Precise Metal Nanoclusters. *Adv. Mater.* **2020**, 1905488

(34) Sugiuchi, M.; Shichibu, Y.; Konishi, K. An Inherently Chiral Au_{24} Framework with Double-Helical Hexagold Strands. *Angew. Chem. Int. Ed.* **2018**, 57, 7855– 7859.

(35) Zhu, Y.; Wang, H.; Wan, K.; Guo, J.; He, C.; Yu, Y.; Zhao, L.; Zhang, Y.; Lv, J.; Shi, L.; Jin, R.; Zhang, X.; Shi, X.; Tang, Z. Enantioseparation of $Au_{20}(PP_3)_4Cl_4$ Clusters with Intrinsically Chiral Cores. *Angew. Chem. Int. Ed.* **2018**, *57*, 9059– 9063.

(36) Chen, S.; Wang, S.; Zhong, J.; Song, Y.; Zhang, J.; Sheng, H.; Pei, Y.; Zhu, M. The Structure and Optical Properties of the $[Au_{18}(SR)_{14}]$ Nanocluster. *Angew. Chem. Int. Ed.* **2015**, *54*, 3145-3149.

(37) Das, A.; Liu, C.; Byun, H. Y.; Nobusada, K.; Zhao, S.; Rosi, N. L.; Jin, R. Structure Determination of $[Au_{18}(SR)_{14}]$. *Angew. Chem. Int. Ed.* **2015**, *54*, 3140-3145.

(38) Tlahuice-Flores, A. New Polyhedra Approach to Explain the Structure and Evolution on Size of Thiolated Gold Clusters. *J. Phys. Chem. C* **2019**, *123*, 10831– 10841.

(39) Tlahuice-Flores, A. Ligand effects on the optical and chiroptical properties of the thiolated Au_{18} cluster. *Phys. Chem. Chem. Phys.* **2016**, *18*, 27738-27744.

(40) Tlahuice-Flores, A.; Whetten, R. L.; Jose-Yacaman, M. Ligand Effects on the Structure and the Electronic Optical Properties of Anionic $Au_{25}(SR)_{18}$ Clusters. *J. Phys. Chem. C* **2013**, *117*, 20867–20875.

(41) Provorse, M. R. and Aikens, C. M. Origin of Intense Chiroptical Effects in Undecagold Subnanometer Particles. *JACS.* **2010**, 132, 4, 1302-1310.

(42) Jiang, W.; Gao, Y.; Xu, D.; Liu, F.; Wang, Z. Structural Influence on Superatomic Orbitals of Typical Gold Nanostructure Building Blocks. *Journal of Electronic Materials* **2017**, 46, 7, 3938-3941.

TOC Figure:

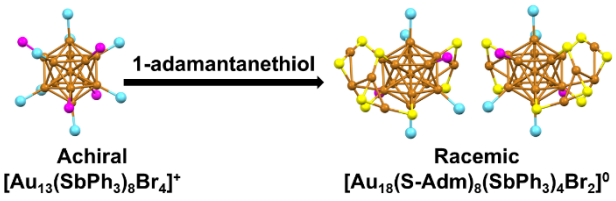
1-adamantanethiol
Achiral
$[Au_{13}(SbPh_3)_8Br_4]^+$
Racemic
$[Au_{18}(S\text{-}Adm)_8(SbPh_3)_4Br_2]^0$